Biosensors and Bioelectronics 126 (2019) 501–509

Contents lists available at ScienceDirect

Biosensors and Bioelectronics

journal homepage: www.elsevier.com/locate/bios

Rapid detection of *Escherichia coli* using fiber optic surface plasmon resonance immunosensor based on biofunctionalized Molybdenum disulfide (MoS_2) nanosheets

Siddharth Kaushik[a,b], Umesh K. Tiwari[a,b], Sudipta S. Pal[a,b], Ravindra K. Sinha[a,c,*]

[a] *Advanced Materials and Sensors (V 4), CSIR-Central Scientific Instruments Organization, Chandigarh 160030, India*
[b] *Academy of Scientific and Innovative Research, CSIR-CSIO Campus, Chandigarh 160030, India*
[c] *TIFAC-Centre of Relevance and Excellence in Fiber Optics and Optical Communication, Department of Applied Physics, Delhi Technological University, Delhi 110042, India*

ARTICLE INFO

Keywords:
Fiber optic sensor
Surface plasmon resonance (SPR)
Molybdenum disulfide (MoS_2) nanosheets
Escherichia coli (*E. coli*)
Label-free immunosensor

ABSTRACT

The molybdenum disulfide (MoS_2) nanosheets functionalized fiber optic surface plasmon resonance (SPR) immunosensor has been reported for the sensitive detection of *Escherichia coli* (*E. coli*). The MoS_2 nanosheets were prepared by chemical exfoliation method. The synthesised nanostructures were characterized for their structural, morphological and optical properties. The *E. coli* monoclonal antibodies were successfully immobilized on the MoS_2 functionalized sensing platform via hydrophobic interactions. An alternative method simplifying the antibodies immobilization process by functionalization of 2D nanomaterial (MoS_2 nanosheets) for rapid (~15 mins) bacterial quantification is presented in this study. The immunosensor uses wavelength interrogation method and a strong linear relationship (R^2 = 0.994) was observed between spectral response of immunosensor and different concentration of *E. coli*. The nonspecificity and cross-reactivity studies of the developed immunosensor were investigated with detection of *Salmonella Typhimurium* and *Staphylococcus aureus*. To demonstrate the practical application, spiked samples of water and orange juice were analysed with acceptable recovery results. The label-free immunosensor exhibits better performance, detection limit (94 CFU/mL), high sensitivity (2.9 nm/1000 CFU mL^{-1}; 3135 nm/RIU) and profound specificity as compared to conventional fiber optic SPR sensor (detection limit: 391 CFU/mL, sensitivity: 0.6 nm/1000 CFU mL^{-1}; 1646 nm/RIU). This sensing platform shows promising applications in regular water and food quality monitoring for various pathogenic microorganisms.

1. Introduction

Waterborne and contaminated food diseases caused by the pathogenic bacteria are public health concern worldwide (Ashbolt, 2004; Flint et al., 2005). According to the WHO reports 2015, the global burden of foodborne illness was 33 million Disability Adjusted Life Years (DALYs) and 40% of the reported cases were from the children below the age of five years (Havelaar et al., 2015). Pathogenic strains of *E. coli*, *Listeria monocytogenes, Salmonella Typhimurium* and *Campylobacter* species are major foodborne pathogens associated with high morbidity and mortality (Altekruse et al., 1997; Tauxe, 2002).

Some serotypes of *E. coli* are non-pathogenic; however, several strains including *E. coli O157: H7*, *E. coli O153:H2* and *E. coli O92: H33* can cause severe foodborne diseases like diarrhoea and acute gastroenteritis (Kaper et al., 2004). Generally, *E. coli* contamination occurs by ingesting of polluted water, unpasteurized milk, contamination meat and food products (Wells et al., 1991; Zhao et al., 2001). The development of label-free, sensitive, and rapid techniques for detection of pathogenic bacteria is also essential for environmental monitoring and in the formulation of food safety policies (Leonard et al., 2003). Conventional culture-based methods for *E. coli* detection involves selective enrichment, isolation and plating followed by biochemical tests which is time consuming and tedious (Wu et al., 2015). Despite providing a highly sensitive and selective platform for *E. coli* detection, well established modern techniques comprising enzyme-linked immunosorbent assay (ELISA) and polymerase chain reaction (PCR) have challenges like complicated sample pre-treatment, requirement of trained personnel and expensive processes (Bonetta et al., 2016). The advent of biosensor technology has improved the food testing process by the development of rapid and sensitive platforms including Surface

* Corresponding author at: Advanced Materials and Sensors (V 4), CSIR-Central Scientific Instruments Organization, Chandigarh 160030, India.
E-mail addresses: dr_rk_sinha@yahoo.com, director@csio.res.in (R.K. Sinha).

https://doi.org/10.1016/j.bios.2018.11.006
Received 2 June 2018; Received in revised form 29 September 2018; Accepted 3 November 2018
Available online 05 November 2018
0956-5663/

enhanced Raman spectroscopy (Srivastava et al., 2015), and prism-based SPR biosensors (Waswa et al., 2007) for the detection of *E. coli*.

Fiber optic sensors comprising long period grating (Deep et al., 2012; Kaushik et al., 2016a, 2016b; Queirós et al., 2014; Tripathi et al., 2012; Tyagi et al., 2018), fiber bragg grating (Srinivasan et al., 2017; Tiwari and Kaushik, 2017) have been explored for surfeit of applications including disease diagnostics and environmental monitoring. Since its inception in 1993 for refractive index measurements, fiber optic SPR sensors have been extensively persuaded in sensing of different biological species (Baliyan et al., 2013; Shrivastav et al., 2015) and chemical compounds (Mishra et al., 2014; Tabassum and Gupta, 2015).

The principle of SPR sensor is based on charge density oscillations at the metal-dielectric interface. These are also known as surface plasma oscillations. Surface Plasmon is the quantum of surface plasma oscillations with transverse-magnetic (TM)-polarized electric field which decay exponentially in both directions having dielectric and metal layer (Homola, 1997). The resonant wavelength is very sensitive to changes in the refractive index of the medium adjacent to the metal layer supporting surface plasmons. Phase matching between the propagating electromagnetic waves and natural oscillating frequencies of free electron of metal layer results in excitation of surface plasmons. The SPR phenomenon occurs at a particular wavelength (resonance wavelength) when propagation constant (K_{ij}) of incident light wave couples with the Surface Plasmon wave propagation constant (K_{sp}) of the conduction band of metal layer (Sharma et al., 2007; Usha and Gupta, 2017). The phase matching condition for the excitation of Surface Plasmon wave is given by

$$\frac{\omega}{\upsilon_p} n_c \sin\theta = \frac{\omega}{\upsilon_p}\left(\frac{n_s^2 \varepsilon_m}{n_s^2 + \varepsilon_m}\right)^{1/2} \quad (1)$$

In Eq. (1), the expression on the left side is the propagation constant of light where ω denotes the angular frequency of incident light and υ_p is the phase velocity of the light wave. While, the right side of the equation represents the real part of the surface plasmon propagation constant with ε_m as the dielectric constant of the metal layer, n_c is the refractive index of core and n_s is the refractive index of surrounding layer.

The generation of SPR leads to sharp dip in the intensity of the transmitted light due to the exponential decay of the energy transfer field intensity of surface plasmon wave (SPW). Therefore, variations in the refractive index at the sensor surface within the SPW region induced by the interaction between biomolecular recognition element (e.g. antibodies, aptamers, lectins etc.) interfaced on the sensor surface and target analytes in samples may bring characteristic changes in resonant wavelength. Albeit fiber optic based sensing techniques are label-free, rapid, and sensitive, they face major predicament in surface bio functionalization process. Primarily in the bio functionalization method, several time-consuming steps are required which limits the sensor prospects for commercialization and large-scale production.

In recent years, many fiber optic immunosensors based on surface modifications with nanomaterials have been reported to improve the sensitivity and biocompatibility of sensing platforms (Kant et al., 2017; Nayak et al., 2017; Singh et al., 2015; Usha and Gupta, 2018; Verma et al., 2011; Yilmaz et al., 2015). The selection and integration of the transducer component with the sensing platform should be one of the most critical factors among all the variables. In this regard, the development of fiber optic SPR immunosensor interfaced with MoS_2 nanosheets that can simplify the biofunctionalization process has been investigated. MoS_2 is made up of three atomic layers having molybdenum layer sandwiched between two sulfur layers, with strong molecular intralayer bonds (coordination bonds) but weak interlayer bonds, which give rise to their layered structure (Kukkar et al., 2016). The fascinating properties of two-dimensional MoS_2 nanosheets have drawn the considerable attention of scientific communities for extensive research in biosensing applications (Kukkar et al., 2018; Mishra et al., 2016). These properties include high electron mobility, relatively low toxicity, large surface to volume ratio, higher optical absorption efficiency, thermal stability and presence of free sulfur groups for hydrophobic interaction (Zeng et al., 2015). These two-dimensional nanosheets provide higher binding sites for antibody immobilization and elude the use of cross linkers for bio functionalizing process. Generally during exfoliation process, several defects mainly sulfur vacancies arises on the surface or edges of nanosheets. These imperfections have been reported as prospective targets for surface functionalization (P. et al., 2015).

In the present study, we propose the development of MoS_2 nanosheets interfaced fiber optic SPR sensor for the quantitative analysis of *E. coli* bacteria. The experimental strategy was based on anchoring the nanosheets at the surface of the gold coated sensing probe and immobilizing the monoclonal antibodies on the functionalized nanosheets via hydrophobic interactions. The reported study combines the rapid and sensitive response of fiber optic SPR sensors with enhanced sensing properties of the MoS_2 nanostructures, which will accord the immunosensor with substantial advantages apart from presenting its aptness aimed at real-time applications for bacteria detection.

2. Experimental

2.1. Materials and Instruments

Step index multimode optical fiber (Core diameter: 400 ± 8 μm, NA: 0.39) was procured from Thorlabs, USA. 11-Mercaptoundecanoic acid (11-MUA), Triton X-100, N-methyl pyrrolidone (NMP), Rhodamine B, N-(3-Dimethylaminopropyl)-N'-Ethyl carbodiimide hydrochloride (EDC), N-Hydroxysuccinimide (NHS) and Molybdenum disulfide (MoS_2) powder were purchased from Sigma-Aldrich, India. *E. coli* monoclonal antibodies (Ab) were procured from MyBioSource, USA. Hydrofluoric acid (HF) (48%), Bovine serum albumin and Phosphate buffered saline (PBS) (0.1 M; pH 7.2) were obtained from Merck, India. Nutrient broth and nutrient agar were procured from Hi Media, India. *Escherichia coli* (*E. coli*) (MTCC No: 1687), *Salmonella typhimurium* (*S. typhimurium*) (MTCC No: 1251), *Staphylococcus aureus* (*S. aureus*) (MTCC No: 87) were procured from Microbial Type Culture Collection and Gene Bank (MTCC), Institute of Microbial Technology, India. The other reagents used were all of the analytical grades. All the solutions were prepared in deionized water (DI water) > 18 mΩ.cm (specific resistivity) at 25 °C, Millipore.

The ultrasonication assisted exfoliated process of MoS_2 sheets was performed in Bath Sonicator from Labman- Ultrasonic Cleaner LMUC-6 (India) followed by probe sonication with the Probe Sonicator (Wensar-Pro-250, India). Eppendorf-Centrifuge 5804 R (India) was employed for the centrifugation process. The optical characteristics of exfoliated MoS_2 nanosheets were studied by a Varian Cary 5000 UV–Visible spectrophotometer from Agilent Technologies, (USA). Vibration transitions of exfoliated MoS_2 nanosheets were studied by Fourier transform infrared (FTIR) spectroscopy (Nicolet iS10, USA). A thin metallic layer of gold (purity: 99.99%) was deposited on the optical fiber by DC magnetron sputtering instrument (Excel Instruments, India). The Raman spectra were measured using a Raman spectrophotometer (Invia, Renishaw, UK) at an excitation wavelength of 514 nm. The morphological studies of the fabricated immunosensor were done by field-emission scanning electron microscope (FESEM, Hitachi S4800, Japan; applied voltage 2–4 kV). The MoS_2 nanostructures were characterized using a transmission electron microscope (TEM) at accelerating voltage of 200 kV (JEOL 2010, Japan). Compositional analysis was achieved by energy dispersive X-ray spectroscope (EDX) attached to the TEM. The topographic characteristics of synthesised nanostructures were analysed in non-contact mode by atomic force microscopy (AFM) (Park Systems, South Korea). The antibodies

immobilization over the surface of sensing probe was investigated by Confocal laser scanning microscopic (CLSM) (Zeiss, LSM 510, Germany)

2.2. Synthesis of molybdenum disulfide (MoS_2) nanosheets

The MoS_2 nanosheets were extracted using ultrasonication assisted liquid exfoliation technique involving the n-methyl pyrrolidone (NMP) as an organic solvent. In typical process, 30 mg of MoS_2 flakes was added to 10 mL of NMP in a 20 mL beaker and sonicated in ultrasonic bath sonicator for 3 h. Then the dispersion was sonicated for 10 min using probe sonic tip at an output power of 125 W at 25 °C. The tip was pulsed for ON mode (7 s) and OFF mode (5 s) to circumvent the overheating effect. Probe sonication for a short duration was done to further disperse the nanoflakes from stacked layers of MoS_2. The dispersion was centrifuged at 5500 rpm for one hour at 10 °C. The one-third of the supernatant was collected and stored in a glass vial at room temperature for further use.

2.3. Fabrication of optical fiber SPR sensor

2.3.1. Etching process of step index multimode optical fiber

The fiber optic SPR sensor was fabricated in a multimode step-index fiber having a core diameter of 400 μm and the numerical aperture of 0.37. For the development of sensing probe, cladding layer was first thermally removed from the 1 cm central portion of the optical fiber (total length: 15 cm). After removal of the polymer clad layer, the stripped portion of the optical fiber was subjected to the standardized etching process. This was done by exposing the fiber to 48% w/w of HF for 40 min under room temperature conditions (25 °C ± 2 °C). The etching process progressed at an approximate etch rate of 3 μm/minute. As reported in the previous studies, the tapering of the fiber structure provides advantage by intensifying the evanescent field that increases the efficacy to interact with the analyte molecules (Harun et al., 2013; Leung et al., 2007). Subsequently, the etched optical fiber was thoroughly cleaned with deionized water and methanol. Dry conditions were ensured for the storage of the etched sensing probe in a glass desiccator.

2.3.2. Deposition of a thin gold layer on the optical fiber by DC Magnetron sputtering method

The deposition of a thin gold (Au) layer over the etched optical fiber was carried out with a Magnetron Sputtering unit having direct current (dc) sputter source. To ensure a uniform coating, the fiber was rotated for 7 cycles at a speed of 9 rpm inside the chamber. Initially, a layer of chromium (Cr) (~5 nm) was deposited on optical fiber before gold coating for proper adherence of gold layers.

2.4. Modification of the fiber optic SPR sensor with MoS_2 nanosheets (MoS_2/Au/optical fiber)

The gold coated optical fiber SPR sensor was modified with MoS_2 nanosheets by dip coating technique. 1 mL solution of the exfoliated MoS_2 nanosheets was left in contact with the gold coated optical fiber. 8 cycles dip coating process was performed with each cycle was completed by submerging the optical fiber in the suspension of MoS_2 nanosheets for 20 s, followed by its drying for 2 min. Before further use, the MoS_2/Au/optical fiber was annealed for 2 h at 50 °C to ensure the proper robustness of the interfacing of MoS_2 with the gold layer.

2.5. Antibodies immobilization

2 mL of PBS solution (0.1 M; pH 7.2) having *E. coli* monoclonal antibodies concentration of 80 μg/mL was prepared and stored at 4 °C. 1 mL of the prepared solution was incubated with the MoS_2 functionalized sensing probe at 37 °C for 2 h in inert environment. The incubation of antibodies with the sensing probe at optimal conditions results in proper and robust bonding between both the components. This biofunctionalization largely involves physisorption via hydrophobic interactions of the *E. coli* monoclonal antibodies on the basal surface of the MoS_2 nanosheets. After incubation the immunosensor was washed with 50 mM of NaOH three times for removal of unbound molecules. The antibodies immobilized sensing probe was further incubated with 2% BSA solution for 30 min to block the non-specific sites of sensing probe. To explore the sensing feature of the developed biosensor, the biofunctionalized sensing probe was placed in the glass flow cell. The light source and detector were connected to the sensing probe at respective ends.

2.6. Fabrication of conventional fiber optic SPR immunosensor (Ab/Au/optical fiber)

In conventional design, the gold coated optical fiber was modified with 11-MUA by immersing the gold coated fiber in 10 mM ethanolic solution of 11-MUA for 6 h. 10 mM EDC and 20 mM NHS were prepared in 10 mL of PBS (pH 7.2) and 1 mL of this prepared cross-linking solution was incubated with 11-MUA interfaced sensing probe to activate carboxyl groups of the sensing probe followed by the incubation of the *E. coli* monoclonal antibodies (80 μg/mL) at 37 °C for two hours. The carboxy terminated thiol layer of 11-MUA forms covalent bond with the amine groups of antibodies via carbodiimide crosslinker chemistry. The process was continued by a treatment with ethanolamine hydrochloride (1 M) for 1 h to block the residual reacting sites. The conventional fiber optic SPR immunosensor was then washed thoroughly with DI water, air dried, and stored at 4 °C before employing for sensing applications.

2.7. Experimental configuration

The schematic of the experimental arrangement used to study the performance of proposed SPR sensor is shown in Fig. 1. The MoS_2/Au/optical fiber with the immobilized *E. coli* monoclonal antibodies was fixed in a glass flow cell with defined inlet and outlet channels. Polychromatic unpolarized light from Tungsten Halogen Light source (Ocean Optics, HL-2000, wavelength range: 360–2400 nm, Output Power: 6.7 mW) was focused at one end of the sensor. For recording transmission spectrum, a CCD spectrometer (Avantes, ULS2048XL-EVO, Wavelength range: 200–1160 nm, Resolution: 0.09–20 nm) was connected to the other end of the sensor. Initially the dark and blank reference readings were noted for characterizing the immunosensor in the presence and absence of light source. This was done to eliminate the noise signals while characterizing the immunosensor in the presence of target analytes. The spectrometer was connected to the laptop to record the resonance wavelength at varied concentrations of the analytes.

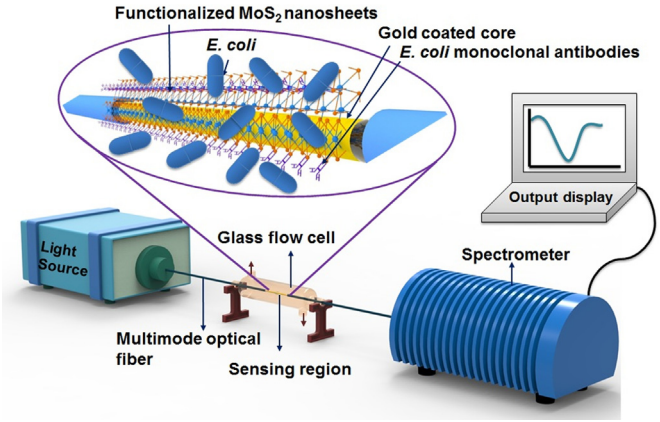

Fig. 1. Schematic representation of the experimental setup of the developed fiber optic SPR immunosensor for the detection of *E. coli*. The interaction time between *E. coli* monoclonal antibodies and *E. coli* sample was 15 min.

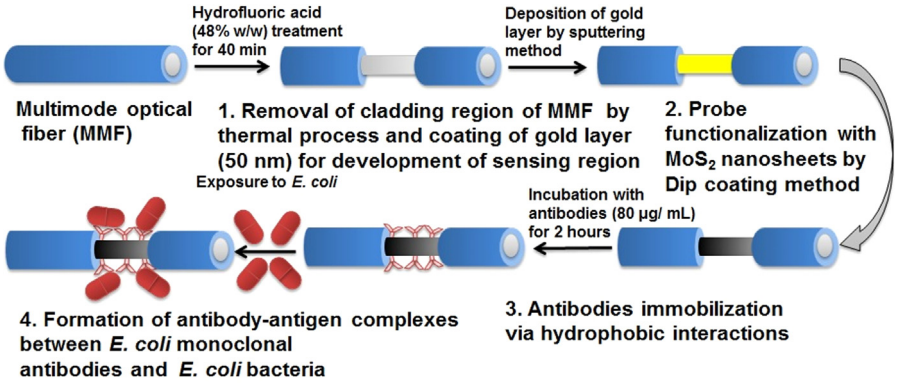

Scheme 1. Schematic depiction of the processes involved in the development of SPR immunosensor with MoS_2 nanosheets as interfacing layer for effective biofunctionalization.

2.8. Quantitative analysis of E. coli

Different concentration of *E. coli* (size ~1–2 µm in length and between 0.5 and 1 µm in diameter) in colony forming unit/ millilitre (CFU/mL) ranging from 1000 CFU/mL to 8000 CFU/mL in 0.1 M PBS buffer (pH 7.2) was prepared. These samples were then allowed to interact with the antibodies (size ~10 nm) immobilized MoS_2/gold/optical fiber immunosensor and the resulting transmission spectra were recorded. All experiments were performed at room temperature (25 °C ± 2 °C). As the intensity-based interrogation method suffers from certain limitations including intensity fluctuation errors by the light source that can lead to false positive results (Blanchard-Dionne et al., 2011). Hence, the optical response of the sensor was based on the wavelength interrogation (in terms of the shift in resonance wavelength), was then correlated with the different tested concentrations of *E. coli*. For each concentration, the experiment was repeated three times. The performance of the MoS_2 nanosheets based developed immunosensor was also compared with a conventionally designed antibodies immobilized gold coated fiber optic SPR immunosensor. The complete process involved in the development of MoS_2 nanosheets based fiber optic SPR immunosensor is shown in Scheme 1.

3. Results and discussion

3.1. Optimization of the gold layer thickness, MoS_2 nanosheets functionalization and antibodies immobilization steps

The thickness of a gold metallic layer significantly influences the performance of the SPR sensor. Therefore, optimizing the thickness of the metal film is essential for better spectral response of the sensor as mentioned in anteceding studies (Suzuki et al., 2008). The gold layers were deposited on optical fiber by magnetron sputtering system for different rotation cycles with definite time intervals. The uniform coating was achieved by continuous rotation of the fiber inside the vacuum chamber by motorized rotor. The fabricated sensing probe with the gold deposition carried for 4, 5, 6 cycles have larger bandwidth compared with fabricated probe with 7 cycles of gold deposition. The larger bandwidth decreases the sensitivity of the fiber optic SPR immunosensor. The sensitivity of sensing probe with 8 rotations of gold deposition has lower sensitivity due to the fact that increase in gold layer thickness decreases the interaction of evanescent wave with the ambient medium. Therefore, the optimal spectral response of fiber optic SPR sensor towards sensing of refractive index (RI) solution (5% v/v glycerol solution RI: 1.338) was observed with optical fiber having 7 rotation cycles of gold deposition as shown in Fig. S1 (a) provided in supplementary information. The thickness of gold deposited uniformly on the surface of optical fiber was 52 ± 3 nm comparable with the thickness reported in previous reports (Iga et al., 2005; Ronot-Trioli et al., 1996).

The influence of the concentration of antibodies on the sensitivity of proposed immunosensor was also investigated. Fig. S1 (b) delineate the outcome of the concentration of antibodies on the spectral response of the Ab/Au/optical fiber towards known concentration of *E. coli* (1000 CFU/mL). The shift in resonance wavelength improved with the increase in concentration of the antibodies from 20 µg/mL to 80 µg/mL, remained approximately constant for 100 µg/mL and then rapidly declined as the concentration of antibodies was further increased. This was probably due to the agglomeration of the antibodies which hindered the antigen binding sites for capturing the target bacteria. Therefore, the concentration of *E. coli* monoclonal antibodies of 80 µg/mL was selected in all experiments.

The interfacing of the MoS_2 nanosheets on the surface of the gold coated optical fiber is a critical step to ensure the efficacy and reproducibility of the subsequent monoclonal antibodies immobilization step. To evaluate the effects of MoS_2 nanosheets thickness on the sensitivity of the SPR spectrum, some preliminary experiments were carried out to realize the best nanostructures anchoring conditions and to avoid surplus aggregation. MoS_2 nanosheets functionalization on gold coated sensing probe was achieved by dip coating method with different cycles (4–12) of deposition. Comparative study for sensitivity response of sensing probes (Ab/MoS_2/Au/optical fiber) with functionalized MoS_2 nanosheets layers of different thickness towards *E. coli* (1000 CFU/mL) solution under optimum conditions is shown in Fig. S1(c). The best response was obtained by sensing probe with MoS_2 nanosheets deposited by dip coating method (eight cycles; thickness: 8 ± 2 nm). For higher cycles of MoS_2 deposition, the insignificant shift in wavelength was recorded when analytes interacted with Ab/MoS_2/Au/optical fiber. The increase in thickness of MoS_2 layers causes aggregation of nanostructures and reduces the interaction of evanescent waves with the antibody-antigen complex, thus lowering the sensitivity of the fiber optic SPR immunosensor.

The pH of the medium has significant influence on formation of antibody-antigen immunocomplex and in immobilization of antibodies on the surface of sensing probe (Reverberi and Reverberi, 2007). The effect of pH on the interaction of *E. coli* bacteria with immobilized antibodies in terms of shift in resonance wavelength is presented in Fig. S1(d). The result displays the best sensitivity of immunosensor at pH range of 7.0–7.5, however the sensitivity decreases with alteration in the pH from this range. It is possibly due to the conformational changes in the antibody structure affecting the immunoassay. Hence the pH range 7.0–7.5 was optimal for the immunological reaction, and all experiments were conducted at pH 7.2.

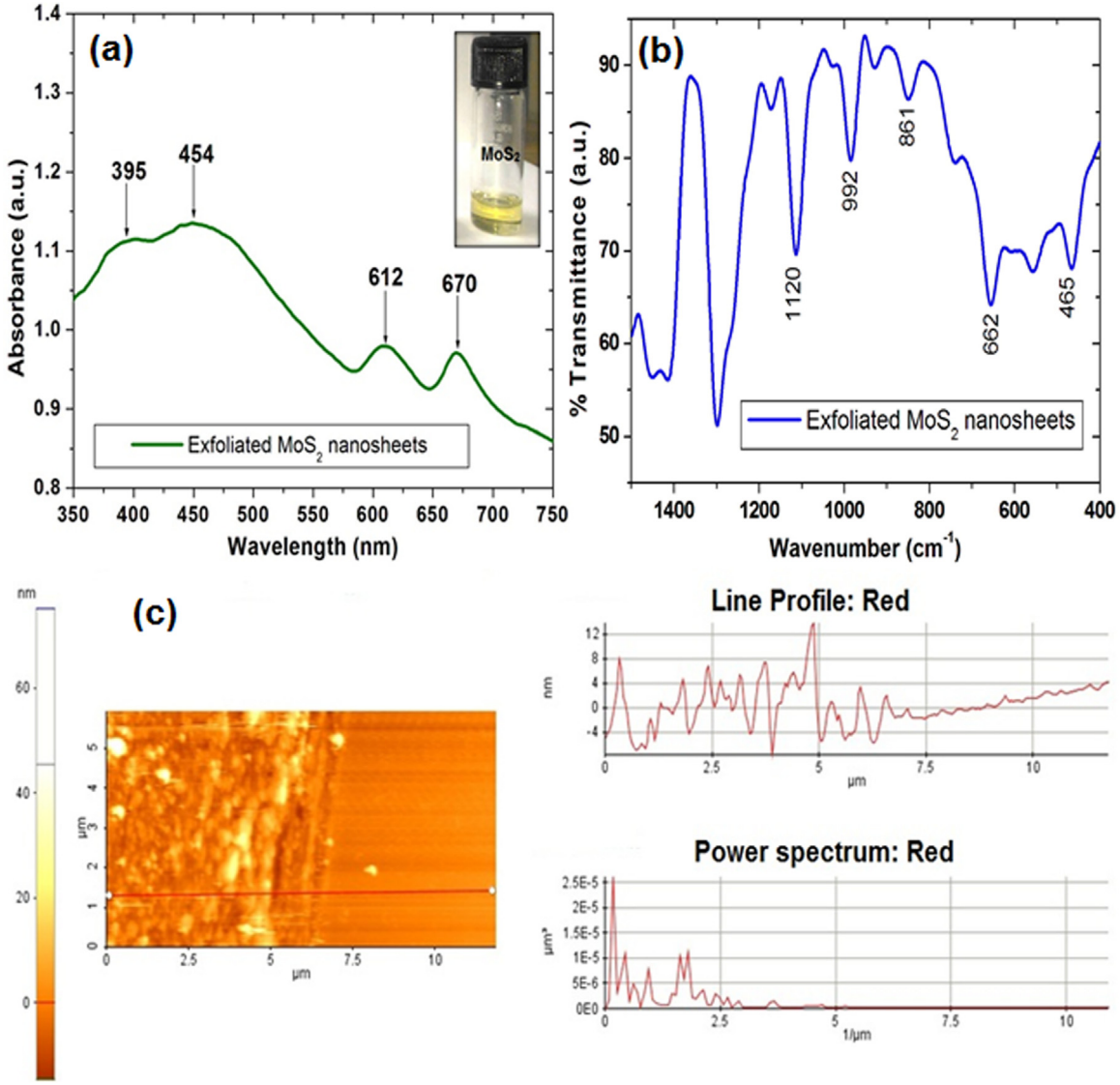

Fig. 2. Spectral analysis: (a) UV–Vis absorption spectra of exfoliated MoS_2 nanosheets. The inset shows homogeneous dispersion of MoS_2 nanosheets in NMP, (b) FTIR spectrum of exfoliated MoS_2 nanosheets, (c) 2D contact mode AFM analysis of MoS2 nanosheets along with the line profile.

3.2. Spectroscopic and morphological characterization of exfoliated MoS_2 Nanosheets and MoS2 functionalized fiber optic SPR sensor

The UV–Vis spectrum of exfoliated MoS_2 nanosheets as shown in Fig. 2(a) presents the characteristics excitonic peaks at 612 nm and 670 nm, originating from the K point of the Brilloium zone. The peaks at 395 and 454 nm due to linear transition of electrons from deep valence band to the conduction band are observed as stated in previous studies (Wilcoxon et al., 1997; Xu et al., 2015). FTIR data provide complementary information on different vibration transitions and several vibrational bands to characterize the synthesised nanosheets. As shown in Fig. 2(b), the characteristic peak at 465 cm^{-1} is attributed to the Mo-S vibration. The peaks a 662 cm^{-1} and 861 cm^{-1} are due to the out-of-plane vibration of sulfur atoms and the vibration of the Mo–S band (Tuteja and Neethirajan, 2017). Owing to the S=O stretch, the peak at 992 cm^{-1} was obtained.

The formation of 2D MoS_2 nanosheets was confirmed by morphological studies using AFM and TEM analysis, which were further supported with EDX analysis (attached with TEM instrument). For the analysis of MoS_2 nanosheets thickness and its homogeneity, atomic force microscopy (AFM) analysis was done using contact mode topography as depicted in Fig. 2(c). For the AFM imaging, the silicon substrate was dip coated with MoS_2 nanosheets and then dried with nitrogen. Typically, the MoS_2 coating on flat substrate was performed by same method as it was carried out on optical fiber. The time of layer deposition on flat substrate was optimized in accordance with the coating of optical fiber. The analysis was carried out using contact mode topography. The study shows the presence of uniformly-sized MoS_2 (8 ± 2 nm) nanosheets.

The ordered lattice and distinctly parallel fringes in TEM images as shown in Fig. 3(a) manifest the crystallinity of the nanostructures. The EDX mapping of the selected area of the copper grid with deposited nanostructures demonstrated the formation of MoS_2 nanosheets as indicated by red dots of Mo and green dots of S in Fig. 3(b). Their overlapping shows uniform stoichiometric distribution of both the elements. The elemental proportion of Molybdenum: Sulfur was roughly in the ratio of 1:2 as displayed in the figure. To probe the elemental composition, EDX elemental analysis of MoS_2 nanosheets with the characteristics peaks of molybdenum, sulfur and copper is shown in Fig. 3(c). Thus, the formation of MoS_2 nanosheets has been comprehensively shown by the different spectroscopic and microscopic characterizations. The morphological characterization of sensing probe with functionalized MoS_2 nanosheets was studied by FESEM analysis as depicted in Fig. 3(d) and (e). Surface modifications are apparent. It is

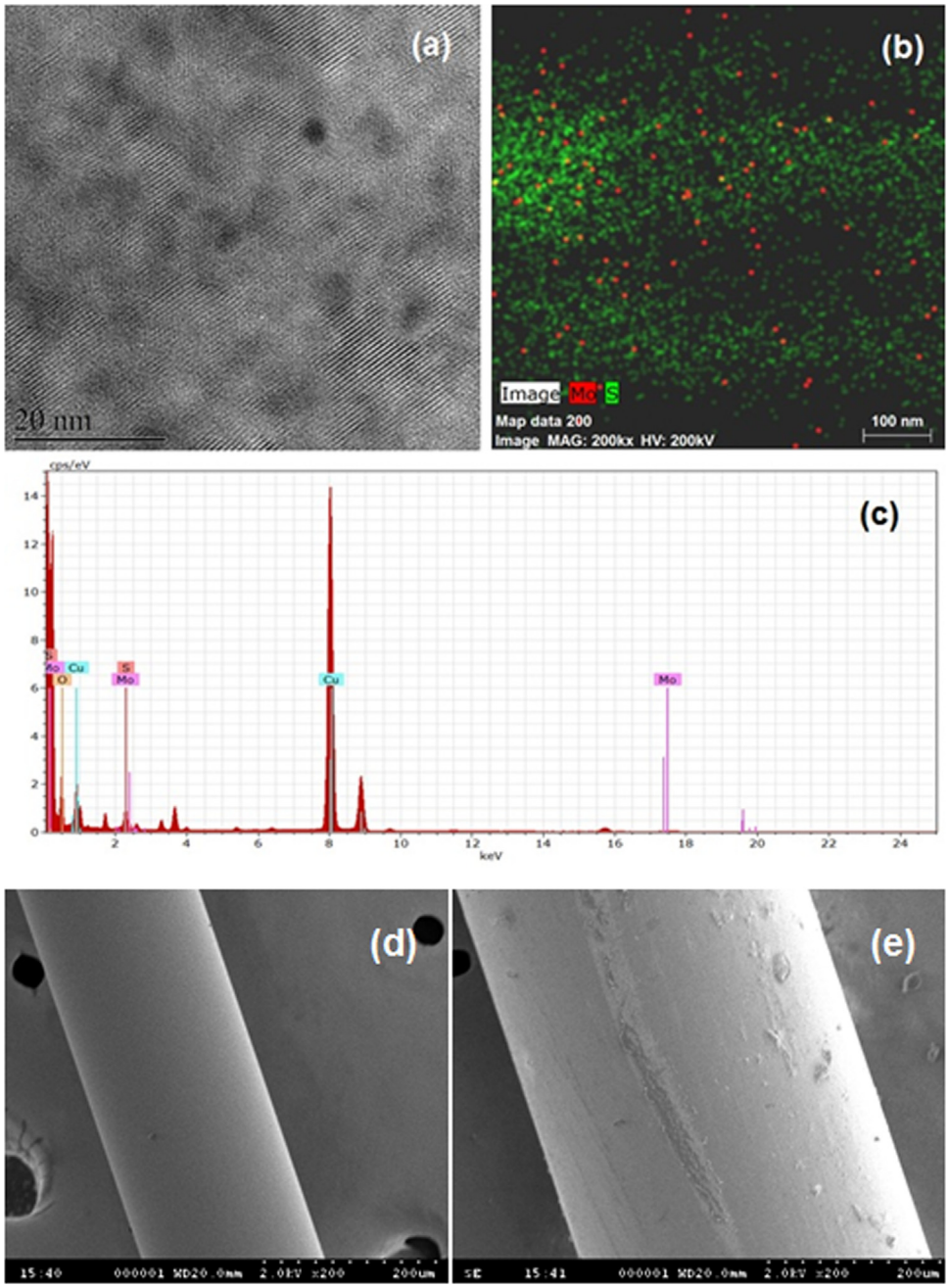

Fig. 3. (a) Transmission electron microscope image of exfoliated MoS_2 nanosheets, (b) elemental mapping displaying the distribution of molybdenum and sulfur element, (c) EDX spectrum of MoS_2 nanosheets, FESEM image of (d) Au/optical fiber and (e) MoS_2/Au/optical fiber. The functionalization of MoS_2 nanosheets is evident from the appearance of coarse particles over the surface of the selected area.

also clear that the protocols used for the nanosheets functionalization produce uniform and well adhered MoS_2 layers.

Raman spectroscopy is a non-destructive technique to determine the physical characteristics and thickness of the material. Raman spectroscopic analysis was done to measure the electronic and vibrational states of synthesised MoS_2 nanosheets. The breathing modes and shear modes (interlayer vibrational modes) in MoS_2 display well established thickness dependence. The intensity and frequency shift of both modes is function of layer thickness. The peak position of in-plane (E^1_{2g}) and out-of-plane (A_{1g}) modes provides precise identification of individual and few layers of MoS_2 (Gopalakrishnan et al., 2014; Zhao et al., 2013). The laser power was selected at minimum level to avoid heating effect and damages caused by laser to nanomaterials. The Fig. 4(a) depicts the Raman spectrometric analysis of exfoliated nanosheets along with MoS_2 nanosheets functionalized sensing probe. As compared to MoS_2 powder, the frequency shift in the vibration modes of the exfoliated MoS_2 sample was observed. The A_{1g} peak is blue-shifted from 408.7 cm^{-1} to 405.2 cm^{-1} while E^1_{2g} peak was red shifted from 381.8 cm^{-1} to 384.7 cm^{-1} which is similar to previous studies (Li et al., 2012; Plechinger et al., 2012; X. Zhang et al., 2015). Raman analysis was also done for confirmation of MoS_2 nanosheets functionalization on gold coated fiber as shown by red spectrum. The characteristic in-plane E^1_{2g} (~384.6 cm^{-1}) and out-of-plane A_{1g} (~405.5 cm^{-1}) vibrational modes were in accordance with standard exfoliated MoS_2. These nanosheets were further explored for the fabrication of a fiber optic SPR immunosensor and the functionalization of MoS_2 nanosheets over the sensing probe was also confirmed by the Raman analysis with prominent E^1_{2g} and A_{1g} shown in purple spectrum. The confocal imaging was done by confocal laser

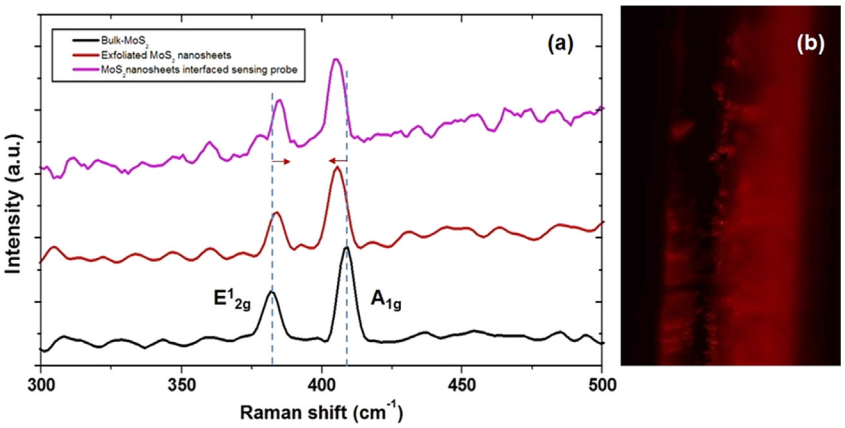

Fig. 4. (a) Raman spectrum of bulk MoS_2 powder (indicated by black color spectra), exfoliated MoS_2 nanosheets (indicated by red color spectra), MoS_2 nanosheets interfaced gold coated fiber optic sensing probe (shown by purple color spectra). The samples were excited by 514 nm laser in the ambient environment at room temperature, (b) Confocal laser scanning microscopic (CLSM) analysis of rhodamine b/E. coli monoclonal antibodies immobilized fiber optic sensing probe.

scanning microscopic (CLSM) to confirm the immobilization of antibodies over the surface of sensing probe. The homogenous fluorescence signals originating from the rhodamine b/*E. coli* antibodies/MoS_2/Au/optical fiber as shown in Fig. 4(b) of CLSM analysis confirms the successful immobilization of antibodies over MoS_2 coated sensing probe. As a control experiment, sensing probes without antibodies were also monitored by CLSM under the similar conditions. The fluorescent signal was not detected. Hence, the observed fluorescence in the sensing probe can be accredited to the presence of E. coli monoclonal antibodies.

The dip coating of the gold coated optical fiber with MoS_2 nanosheets dispersion resulted in uniform interfacing of the nanomaterial on the gold coated fiber as verified with scanning electron microscopy and Raman spectroscopy. From these characterization results, it is anticipated that the adequately interfaced MoS_2 nanosheets should provide higher surface area for immobilization of antibodies.

3.3. Comparative study of response characteristics

To study the spectral characteristics of the fiber optic SPR sensor, transmission spectra were obtained for five different concentrations of *E. coli* in phosphate buffer solution with a conventional SPR sensor and MoS_2 functionalized SPR immunosensor. The resonance wavelength attained after the antibodies immobilization was considered as reference peak. The SPR spectra of varying concentration of *E. coli* ranging from 1000 CFU/mL to 8000 CFU/mL in 0.1 M PBS (pH 7.2) obtained from conventional sensor is shown in Fig. 5(a). All the SPR spectra were recorded after 15 min of adding the solution in the flow cell. It can be observed that the resonance dip in the SPR spectrum shows red shifts as the concentration of *E. coli* increases. The resonance wavelength (wavelength corresponding to minimum transmitted power) was determined for each concentration. Fig. 5(c) shows the corresponding shift in the resonance wavelength with concentration of *E. coli* by Ab/MoS_2/Au/optical fiber. From the error bar graph depicted in Fig. 5(b) and (d), it can be observed that the resonance wavelength increases linearly with the concentration of *E. coli* in the range of 1000 CFU/mL to 8000 CFU/mL in both Ab/Au/optical fiber and Ab/MoS_2/Au/optical fiber. For each concentration, the experiment was performed three times. The sensing probe was cleaned with 0.01% Triton X-100 in deionised water after each experiment. The change in the resonance wavelength was due to the fact that when *E. coli* bacteria interact with *E. coli* monoclonal antibody immobilized over the gold layer in conventional sensor and over the MoS_2 functionalized developed SPR immunosensor, the formation of antibody-antigen complex changes the ambient refractive index and tune the properties of the interacting evanescent wave. The change in the refractive index is directly proportional to the concentration of *E. coli* in buffer solution. This difference in refractive index is marked by red shift in resonance wavelength of the transmission (SPR) spectra. The extent of wavelength shift is greater in the Ab/MoS_2/Au/optical fiber demonstrating better sensor sensitivity. The large surface area of functionalized nanosheets increases the binding density of antibodies which results in capturing more target analytes (*E. coli*). It should also be noted that the MoS_2 monolayer has higher refractive index (4.49@ λ = 651 nm) (H. Zhang et al., 2015) as compared to gold layer. The MoS_2 nanosheets with large RI sustain evanescent waves for smaller thicknesses. The thin layer (8 ± 2 μm) of these nanosheets permits large proportion of evanescent field in the biorecognition region. As the sensitivity depends on the overlap integral of the electrical intensity in the ambient analyte region related to the interaction volume (Shalabney and Abdulhalim, 2011), the higher interaction of guided wave and analytes increases the sensitivity of the immunosensor. It was observed that the developed Ab/MoS_2/Au/optical fiber immunosensor provide better detection sensitivity 2.9 nm/1000 CFU mL^{-1} [(determined by the gradient of the regression line equation) with R^2 = 0.994] than conventional fiber optic SPR immunosensor (0.6 nm/1000 CFU mL^{-1} with R^2 = 0.996). The sensitivity was also measured in terms of shift in resonance wavelength per unit change in refractive index as denoted by (nm/RIU) and it was observed to be 3135 nm/RIU for the developed SPR immunosensor as compared to 1646 nm/RIU of the conventional SPR immunosensor. The calculated limit of detection (LOD) [defined by 3*SD_{Blank}/slope of calibration curve (Bhardwaj et al., 2017) with the developed SPR immunosensor of 94 CFU/mL was better as compared to the LOD of 391 CFU/mL with conventional design.

4. Conclusion

In summary, the present study provides significant senstivity enhancement and improvement in biofunctionalization of fiber optic immunosensors, particularly SPR immunosensor for rapid analysis of pathogens. This work demonstrates the simplistic synthesis of MoS_2 nanosheets which was confirmed by morphological and spectral studies using UV–Vis analysis, FTIR, AFM and TEM with EDX analysis. The exfoliated nanosheets were interfaced with gold coated SPR immunosensor through the Au-S bonds and then effectively bioconjugated with *E. coli* monoclonal antibodies via hydrophobic interactions. The biofunctionalization of the developed sensing probe with *E. coli* monoclonal antibodies was confirmed by confocal microscopy, raman spectroscopy and FESEM analysis. The label free detection of *E.coli* (1000 CFU/mL–8000 CFU/mL) was achieved with high precision. It was demonstrated that the present sensing platform can sensitively detect *E. coli* as low as 94 CFU/mL. The target analyte (*E. coli*) has been selectively detected by the developed immunosensor even in the presence of interfering bacteria. However, the developed fiber optic SPR system has certain limitations including high-cost, decrease in performance due to instability of the antibodies after certain time interval and lengthy gold deposition process to support the surface plasmon wave. The sensing processes are needed to be explored which can increase the sensor's stability and robustness. The developed sensor can be

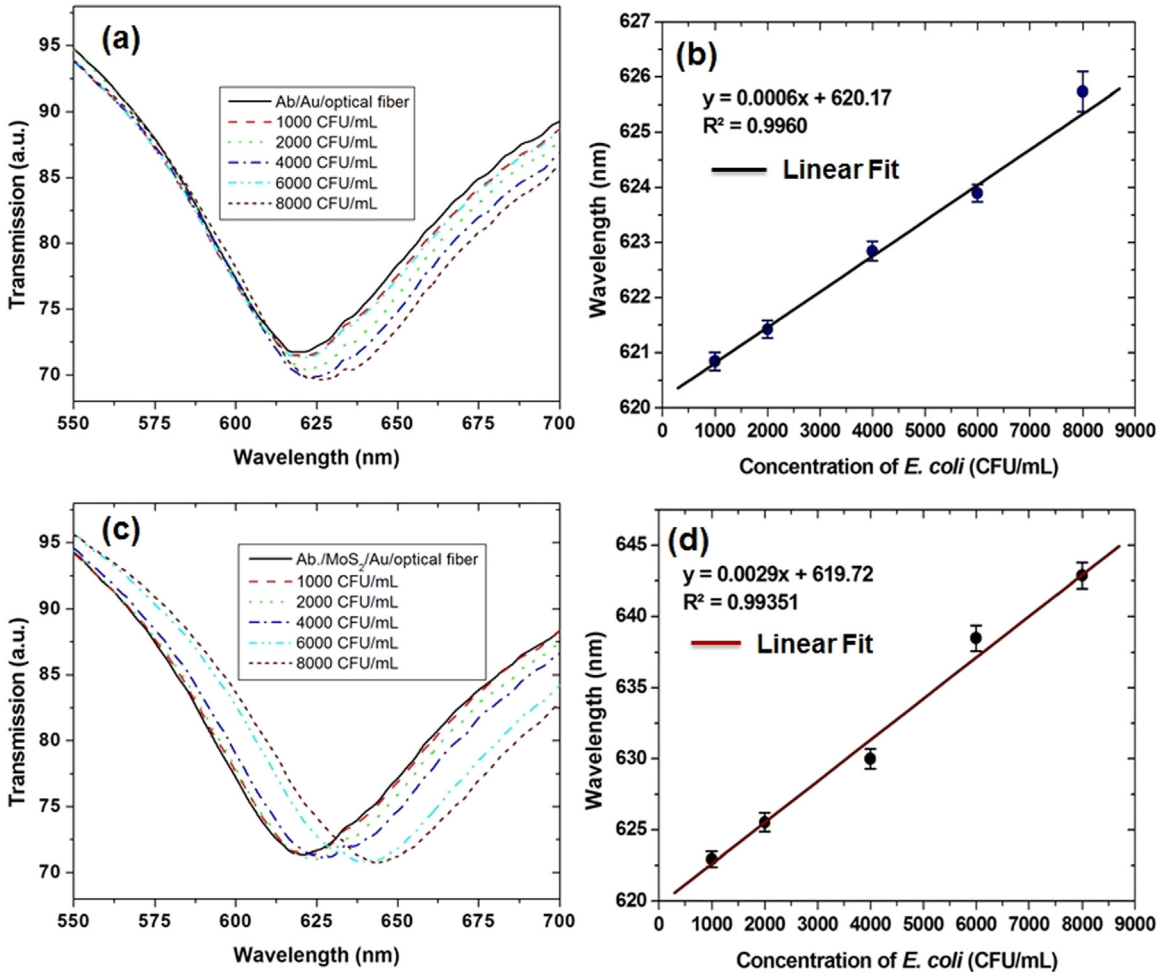

Fig. 5. (a) Transmission spectrum of Ab/Au/optical fiber immunosensor for *E. coli* concentration (1000 CFU/mL to 8000 CFU/mL), (b) corresponding shift in resonance wavelength of Ab/Au/optical fiber immunosensor vs. concentrations of *E. coli* along with standard deviation as error bars, (c) transmission spectra of Ab/MoS_2/Au/optical fiber immunosensor depicting resonance wavelengths corresponding to the different concentration of *E. coli,* (d) variation of resonance wavelength vs. concentrations of *E. coli* along with standard deviation as error bars for developed immunosensor.

potentially explored for the real-time monitoring of water and food products even at remote locations.

Acknowledgements

The authors acknowledge the financial support provided by Council of Scientific and Industrial Research (EMR 0001) and University Grants Commission, New Delhi) for the present study. The authors are grateful to Mrs. Nilima at the Department of Statistics, Manipal Academy of Higher Education, Karnataka for helping in statistical analysis. The authors are thankful to Dr. A.K. Paul, Ms. Aditi, Dr. Udaybir Singh Abhishek Grain and Kamalpreet Singh of CSIO for fruitful discussion. The authors sincerely express gratitude to Dr. Kiran S. Hazra and Ms. Renu Rani at INST, Mohali for TEM and EDS analysis.

Conflicts of interest

The authors declare that they have no conflicts of interest.

Appendix A. Supporting information

Supplementary data associated with this article can be found in the online version at doi:10.1016/j.bios.2018.11.006.

References

Altekruse, S., Cohen, M., Swerdlow, D., 1997. Emerg. Infect. Dis. 3 (3), 285.
Ashbolt, N.J., 2004. Toxicology 198 (1–3), 229–238.
Baliyan, A., Bhatia, P., Gupta, B.D., Sharma, E.K., Kumari, A., Gupta, R., 2013. Sens. Actuators B: Chem. 188, 917–922.
Bhardwaj, N., Bhardwaj, S.K., Mehta, J., Kim, K.-H., Deep, A., 2017. ACS Appl. Mater. Interfaces 9 (39), 33589–33598.
Blanchard-Dionne, A., Guyot, L., Patskovsky, S., Gordon, R., Meunier, M., 2011. Opt. Express 19 (16), 15041–15046.
Bonetta, S., Pignata, C., Lorenzi, E., De Ceglia, M., Meucci, L., Bonetta, S., Gilli, G., Carraro, E., 2016. Environ. Sci. Pollut. Res. 23 (15), 15302–15309.
Deep, A., Tiwari, U., Kumar, P., Mishra, V., Jain, S.C., Singh, N., Kapur, P., Bharadwaj, L.M., 2012. Biosens. Bioelectron. 33 (1), 190–195.
Flint, J.A., Van Duynhoven, Y.T., Angulo, F.J., DeLong, S.M., Braun, P., Kirk, M., Scallan, E., Fitzgerald, M., Adak, G.K., Sockett, P., 2005. Clin. Infect. Dis. 41 (5), 698–704.
Gopalakrishnan, D., Damien, D., Shaijumon, M.M., 2014. ACS Nano 8 (5), 5297–5303.
Harun, S., Lim, K., Tio, C., Dimyati, K., Ahmad, H., 2013. Opt.-Int. J. Light Electron Opt. 124 (6), 538–543.
Havelaar, A.H., Kirk, M.D., Torgerson, P.R., Gibb, H.J., Hald, T., Lake, R.J., Praet, N., Bellinger, D.C., De Silva, N.R., Gargouri, N., 2015. PLoS Med. 12 (12), e1001923.
Homola, J., 1997. Sens. Actuators B: Chem. 41 (1–3), 207–211.
Iga, M., Seki, A., Watanabe, K., 2005. Sens. Actuators B: Chem. 106 (1), 363–368.
Kant, R., Tabassum, R., Gupta, B.D., 2017. Nanotechnology 28 (19), 195502.
Kaper, J.B., Nataro, J.P., Mobley, H.L., 2004. Nat. Rev. Microbiol. 2 (2), 123.
Kaushik, S., Tiwari, U., Kaur, S., Rajesh, Paul, A., Bhatnagar, R., 2016a. AIP Conference Proceedings. AIP Publishing, pp. 020110.
Kaushik, S., Tiwari, U., Saini, T.S., Pandey, A., Paul, A., Sinha, R.K., 2016b. International Conference on Fibre Optics and Photonics. Optical Society of America, pp. Th3A. 59.
Kukkar, M., Mohanta, G.C., Tuteja, S.K., Kumar, P., Bhadwal, A.S., Samaddar, P., Kim, K.-H., Deep, A., 2018. Biosens. Bioelectron.
Kukkar, M., Tuteja, S.K., Sharma, A.L., Kumar, V., Paul, A.K., Kim, K.-H., Sabherwal, P.,

Deep, A., 2016. ACS Appl. Mater. Interfaces 8 (26), 16555–16563.
Leonard, P., Hearty, S., Brennan, J., Dunne, L., Quinn, J., Chakraborty, T., O'Kennedy, R., 2003. Enzym. Microb. Technol. 32 (1), 3–13.
Leung, A., Shankar, P.M., Mutharasan, R., 2007. Sens. Actuators B: Chem. 125 (2), 688–703.
Li, H., Zhang, Q., Yap, C.C.R., Tay, B.K., Edwin, T.H.T., Olivier, A., Baillargeat, D., 2012. Adv. Funct. Mater. 22 (7), 1385–1390.
Mishra, A.K., Mishra, S.K., Verma, R.K., 2016. J. Phys. Chem. C 120 (5), 2893–2900.
Mishra, S.K., Tripathi, S.N., Choudhary, V., Gupta, B.D., 2014. Sens. Actuators B: Chem. 199, 190–200.
Nayak, J.K., Maharana, P.K., Jha, R., 2017. J. Phys. D: Appl. Phys. 50 (40), 405112.
P, N.E., J, C.B., Zhen, O.J., Joel, vE., Della, G.E., C.A, F., S, S.M.J., Serge, Z., Kourosh, Kz, Torben, D., 2015. Adv. Mater. 27 (40), 6225–6229.
Plechinger, G., Heydrich, S., Eroms, J., Weiss, D., Schüller, C., Korn, T., 2012. Appl. Phys. Lett. 101 (10), 101906.
Queirós, R., Gouveia, C., Fernandes, J., Jorge, P., 2014. Biosens. Bioelectron. 62, 227–233.
Reverberi, R., Reverberi, L., 2007. Blood Transfus. 5 (4), 227.
Ronot-Trioli, C., Trouillet, A., Veillas, C., Gagnaire, H., 1996. Sens. Actuators A: Phys. 54 (1–3), 589–593.
Shalabney, A., Abdulhalim, I., 2011. Laser Photonics Rev. 5 (4), 571–606.
Sharma, A.K., Jha, R., Gupta, B.D., 2007. IEEE Sens. J. 7 (8), 1118–1129.
Shrivastav, A.M., Mishra, S.K., Gupta, B.D., 2015. Sens. Actuators B: Chem. 212, 404–410.
Singh, M., Holzinger, M., Tabrizian, M., Winters, Sa, Berner, N.C., Cosnier, S., Duesberg, G.S., 2015. J. Am. Chem. Soc. 137 (8), 2800–2803.
Srinivasan, R., Umesh, S., Murali, S., Asokan, S., Siva Gorthi, S., 2017. J. Biophotonics 10 (2), 224–230.
Srivastava, S.K., Hamo, H.B., Kushmaro, A., Marks, R.S., Grüner, C., Rauschenbach, B., Abdulhalim, I., 2015. Analyst 140 (9), 3201–3209.
Suzuki, H., Sugimoto, M., Matsui, Y., Kondoh, J., 2008. Sens. Actuators B: Chem. 132 (1), 26–33.
Tabassum, R., Gupta, B.D., 2015. Sens. Actuators B: Chem. 220, 903–909.
Tauxe, R.V., 2002. Int. J. Food Microbiol. 78 (1–2), 31–41.
Tiwari, U., Kaushik, S., 2017. Optical Sensing, Imaging, and Photon Counting: Nanostructured Devices and Applications 2017. International Society for Optics and Photonics, pp. 103530Y.
Tripathi, S.M., Bock, W.J., Mikulic, P., Chinnappan, R., Ng, A., Tolba, M., Zourob, M., 2012. Biosens. Bioelectron. 35 (1), 308–312.
Tuteja, S.K., Neethirajan, S., 2017. Chem. Commun. 53 (72), 10002–10005.
Tyagi, D., Mishra, S.K., Zou, B., Lin, C., Hao, T., Zhang, G., Lu, A., Chiang, K.S., Yang, Z., 2018. J. Mater. Chem. B 6 (3), 386–392.
Usha, S.P., Gupta, B.D., 2017. Appl. Opt. 56 (20), 5716–5725.
Usha, S.P., Gupta, B.D., 2018. Biosens. Bioelectron. 101, 135–145.
Verma, R., Gupta, B.D., Jha, R., 2011. Sens. Actuators B: Chem. 160 (1), 623–631.
Waswa, J., Irudayaraj, J., DebRoy, C., 2007. LWT-Food Sci. Technol. 40 (2), 187–192.
Wells, J., Shipman, L., Greene, K., Sowers, E., Green, J., Cameron, D., Downes, F., Martin, M., Griffin, P., Ostroff, S., 1991. J. Clin. Microbiol. 29 (5), 985–989.
Wilcoxon, J., Newcomer, P., Samara, G., 1997. J. Appl. Phys. 81 (12), 7934–7944.
Wu, W., Zhao, S., Mao, Y., Fang, Z., Lu, X., Zeng, L., 2015. Anal. Chim. Acta 861, 62–68.
Xu, S., Li, D., Wu, P., 2015. Adv. Funct. Mater. 25 (7), 1127–1136.
Yilmaz, E., Majidi, D., Ozgur, E., Denizli, A., 2015. Sens. Actuators B: Chem. 209, 714–721.
Zeng, S., Hu, S., Xia, J., Anderson, T., Dinh, X.-Q., Meng, X.-M., Coquet, P., Yong, K.-T., 2015. Sens. Actuators B: Chem. 207, 801–810.
Zhang, H., Ma, Y., Wan, Y., Rong, X., Xie, Z., Wang, W., Dai, L., 2015a. Sci. Rep. 5, 8440.
Zhang, X., Qiao, X.-F., Shi, W., Wu, J.-B., Jiang, D.-S., Tan, P.-H., 2015b. Chem. Soc. Rev. 44 (9), 2757–2785.
Zhao, C., Ge, B., De Villena, J., Sudler, R., Yeh, E., Zhao, S., White, D.G., Wagner, D., Meng, J., 2001. Appl. Environ. Microbiol. 67 (12), 5431–5436.
Zhao, Y., Luo, X., Li, H., Zhang, J., Araujo, P.T., Gan, C.K., Wu, J., Zhang, H., Quek, S.Y., Dresselhaus, M.S., 2013. Nano Lett. 13 (3), 1007–1015.